Chapter 2

Accumulator Rings and Injection Beam Line

Authors and Contributors

Accumulator Rings and Injection Beam Line

Author:

C R Prior[1]

Contributors:

J R J Bennett,[1] M Masullo,[2] S Pape Moller,[3] C R Prior,[1] G.H. Rees,[1] J V Trotman,[1] V Vaccaro,[2] C M Warsop[1]

[1]RAL/ISIS, [2]Univ. Naples, [3]Univ. Aarhus

Contents

Accumulator Rings and Injection Beam Line

2 ACCUMULATOR RINGS AND INJECTION BEAM LINE

2.1 OVERVIEW

The changes made to the design of the rings and injection beam lines over the period 1999-2003 include an increase in ring radius, amendments to the linac chopping requirements, and a reassessment of the parameters for ring injection painting. These were necessary to avoid excessive temperatures in the injection stripping foil while maintaining the good beam distribution that the earlier study had predicted. The changes have all been found to be acceptable. Subsequent work has focussed on improved simulation techniques and reviewed aspects such as the electron cloud problem in the light of developments at other laboratories.

The guiding principle throughout the project has been that the requirement to deliver 5 MW of beam power to the short pulse target can be met through the use of two, 50 Hz, 1.334 GeV accumulator rings. Stacked one above the other, these are filled and emptied successively once every cycle with 2.34×10^{14} protons per ring, and particles are accumulated via a multi-turn charge exchange ring injection process so as to compress the time duration of the linac pulse.

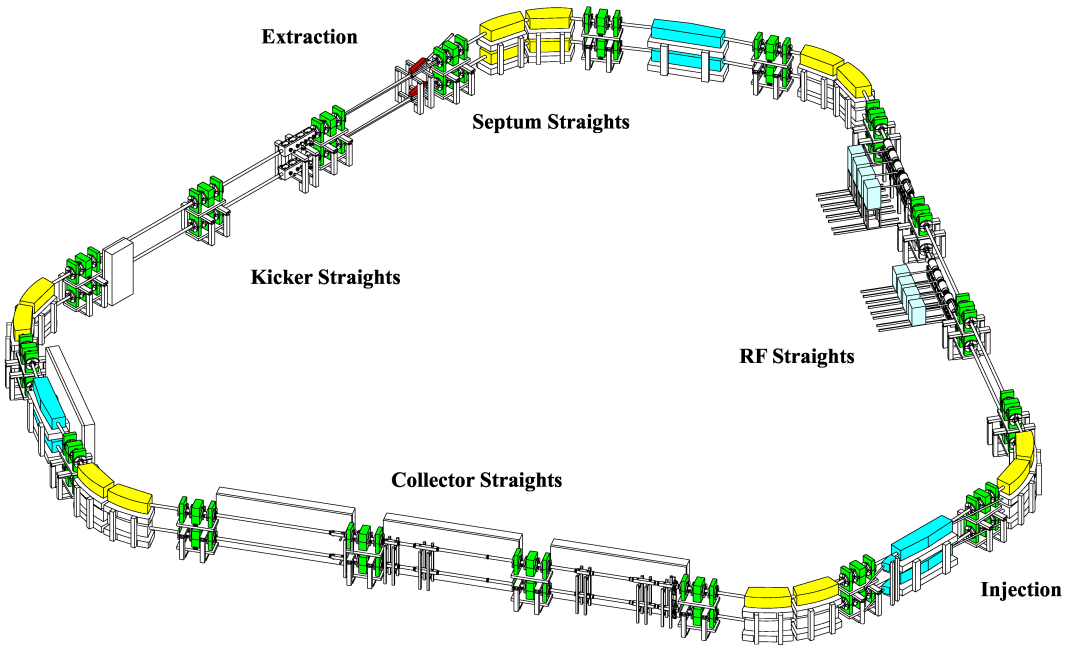

Figure 2.1.1: ESS Stacked Accumulator Rings

Chopping the incoming beam in the low energy stages of the linac (as described in Chapter 1) helps minimise the ring beam losses and reduces radiation damage. A single bunch is accumulated in each ring over 583 injection turns and is contained by combined RF systems of harmonic numbers one and two. After fast ring extraction and a switch magnet, the two bunches in each 50 Hz pulse are transported with bunch and pulse durations of 0.6 and 1.4 μs, respectively, to the short pulse neutron target.

In order to control beam losses, halo scraping is planned in the transfer line from the linac to the rings. The transverse and longitudinal profiles of the beam emerging from the H^- linac are cleaned using a number of stripping foils in a large achromatic 180° bending section. A special injection region is included in the rings to allow combined injection painting in all three phase planes. This reduces the number of proton foil transits (and consequent foil heating) and minimises the uncontrolled beam loss. Elsewhere in the ring, a beam loss collection system is used to localise the particle loss.

Details of the accumulator ring are shown in Figure 2.1.1 and a summary of the main ring parameters is given in Table 2.1.1.

Table 2.1.1: Parameters for the Accumulator Rings ISKG will streamline table

Ring max. kinetic energy (MeV)	1334.0
Repetition frequency (Hz)	50.0
Accumulator ring mean radius (m)	35.0
Ring rms unnorm. emittance (π μrad m)	30.0
Ring average circulating current (A)	46.55
Number of circulating protons ($\times 10^{14}$)	2.34
Revolution frequency (MHz)	1.2416
Main (h) & additional harmonic number	1,2
Peak kV/turn at injection	8 to 26
Ratio V(2h) / (V(h) at injection	0.4 to 0.9
Peak kV/turn during storage	26.0 to 28.0
No of ‘h’ cavities/ring	3 (single gap)
No of ‘2h’ cavities/ring	1 (double gap)
Length of ‘h’ and ‘2h’ cavities (m)	1.5, 2.2
Bunch and pulse extent at target (μs)	0.6, 1.4

2.2 RING BEAM DYNAMICS

Following enlargement of the rings from the original 26 m to 35 m radius, recent studies have centred on a revision of the closed orbit correction scheme and an initial approach to the important issue of electron-proton instability.

2.2.1 Closed Orbit Distortion and Correction

The sensitivity of the enlarged lattice to transverse misalignments, tilts and magnetic field errors has been investigated, together with an orbit correction scheme. Quadrupole transverse misalignments, dipole rotations around the longitudinal axes and dipole field errors have been introduced in the magnetic elements. It has been found that the largest effect is due to the quadrupole misalignments and that a correction scheme may be devised which shows a good balance between the corrected closed orbit deviations and the required correction strengths.

The computer code MAD has been used for generating Gaussian random error distributions in the ring elements and calculating the resulting closed orbit. Twenty different error distributions have been used in each case, and the residual and corrected closed orbit deviation found for the monitor and corrector locations indicated in Figure 2.2.1. 14 horizontal and 15 vertical closed orbit monitors were used, together with 9 additional horizontal-vertical monitors in the injection and extraction regions and the long straight sections. Orbit correctors include 12 horizontal back leg windings on the main lattice dipoles and 14 vertical dipole magnets, each of length 20 cm, installed at 5 cm to one side of each of 14 of the main lattice defocussing quadrupoles.

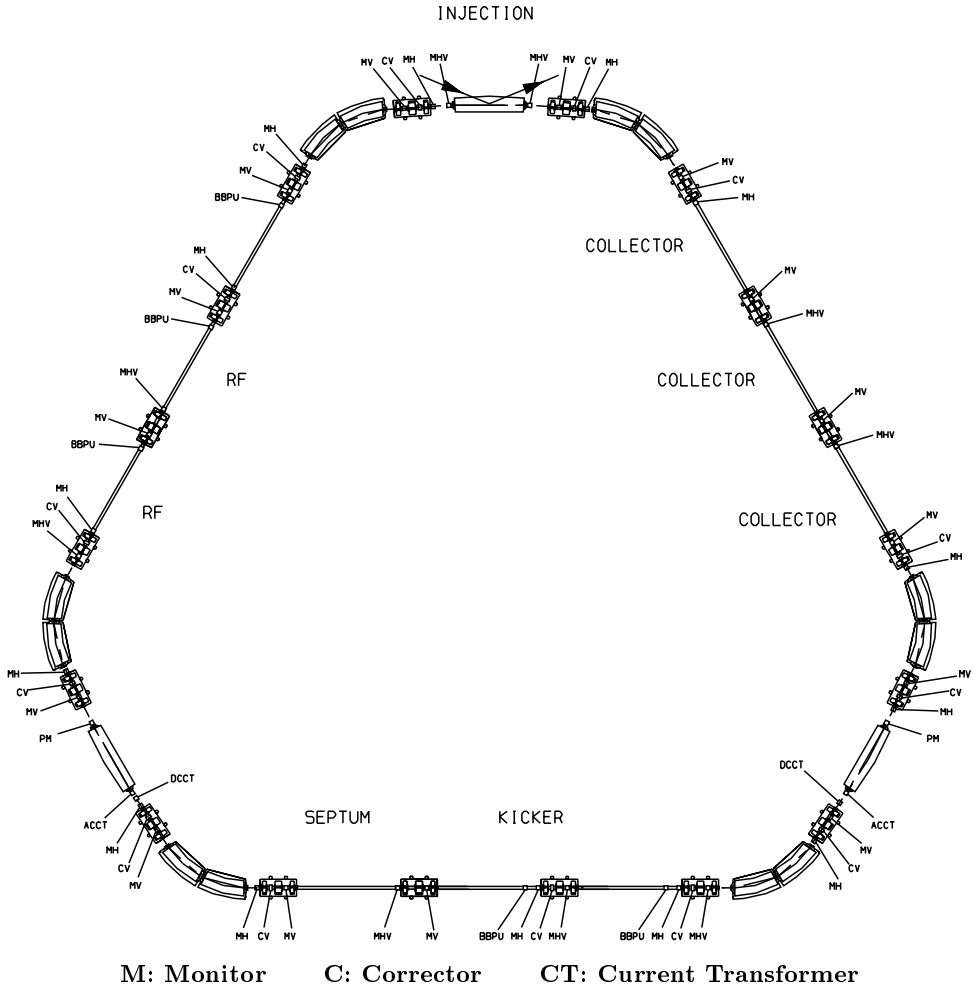

Figure 2.2.1: Closed orbit correction scheme

The rms values assumed for the errors in the computations are $\Delta x = \Delta y = 0.3$ mm for the quadrupole misalignments, $\Delta\varphi = 0.1$ mrad for the dipole rotations and $\Delta B/B = 3\times10^{-4}$ for the relative field errors in the dipoles. The related horizontal and vertical closed orbit deviation around the ring, before and after correction, are given in Table 2.2.1, with their rms values averaged over all the different cases simulated. The related corrector deflection angles are given in the last columns, for horizontal and vertical correctors separately. The upper part of the table assumes monitors without errors, while the lower part assumes monitors with Gaussian distributed read-errors of 0.8 mm rms value in both the Δ_x and Δ_y transverse planes. Maximum orbit displacements after correction are < 0.8 mm for the case of monitor read errors, with maximum corrector strengths of the order of 0.5 mrad in the horizontal plane and 0.2 mrad in the vertical plane.

Table 2.2.1: Uncorrected and corrected closed orbit deviations

RMS errors	Xrms unc. (mm)	Yrms unc. (mm)	Xrms corr. (mm)	Yrms corr. (mm)	α_x (mrad)	α_y (mrad)
Misaligned quads	5.065	5.024	0.557	0.387	0.438	0.191
Dipole fields	2.460	0.0	0.252	0.0	0.164	0.0
Tilted dipoles	~0.0	0.459	~0.0	0.243	0.0	0.019
All	**5.257**	**4.066**	**0.560**	**0.363**	**0.529**	**0.189**
As above + BPM read errors						
Misaligned quads	6.374	5.420	0.740	0.590	0.545	0.196
Dipole fields	2.000	0.741	0.463	0.476	0.273	0.085
Tilted dipoles	0.855	0.946	0.553	0.541	0.215	0.109
All	**4.854**	**5.079**	**0.692**	**0.623**	**0.517**	**0.206**

2.2.2 Beam Stability

In addition to foil scattering and betatron resonances, the beam motion in the accumulators may suffer from single bunch longitudinal and transverse instabilities and electron proton instabilities. The former were discussed in earlier reports and recent work has concentrated on the so-called electron cloud problem, which is a cause for concern at many leading laboratories.

The electron cloud instability is thought to be caused by the interaction of the beam with electrons created inside the vacuum chamber and has only relatively recently been recognised as a limitation to intensity in high power rings. The electrons are formed by ionisation of the residual gas, through proton beam loss or (in some machines, though not in ESS) from the photo-electric effect triggered by synchrotron radiation. Those electrons leaving the trailing edge of a passing proton bunch pass rapidly to the walls and produce copious secondary emission electrons. The yield depends strongly on factors such as the proton beam intensity, bunch spacing, secondary emission coefficients and the gas pressure. The secondary electrons in turn produce tertiaries. Many survive to interact with subsequent bunches and a so-called electron cloud can build up. This has serious implications for beam stability, beam loss and emittance growth.

An instability with the electron cloud features (e-p instability) has been observed at the Proton Storage Ring (PSR) at Los Alamos National Laboratory, where it strongly limits intensity [Macek, 2001]. In contrast, no coasting or bunched beam e-p instability has been found in the ISIS synchrotron, which has similar parameters to the PSR [Rees, 1999]. Several of the distinct features of ISIS are therefore planned for ESS, including beam losses confined to specific collimation areas, large acceptances, low impedance kicker units and possibly rectangular vacuum chambers with profiled walls. Lower vacuum pressures are likely and titanium nitride wall coatings will be used to reduce the secondary electron emission.

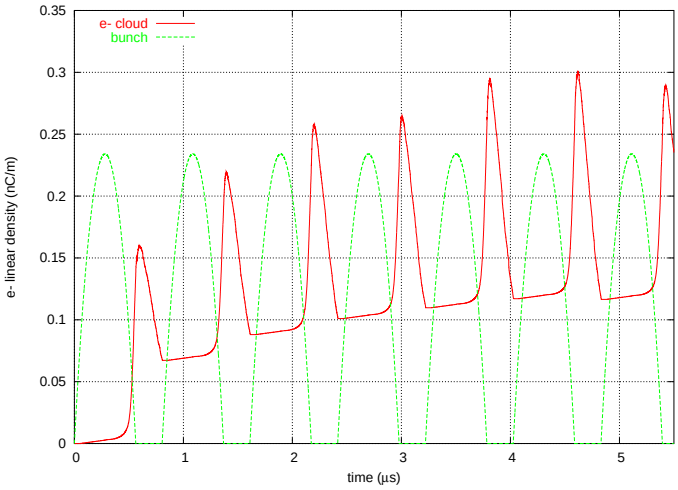

(a) Electron cloud build-up

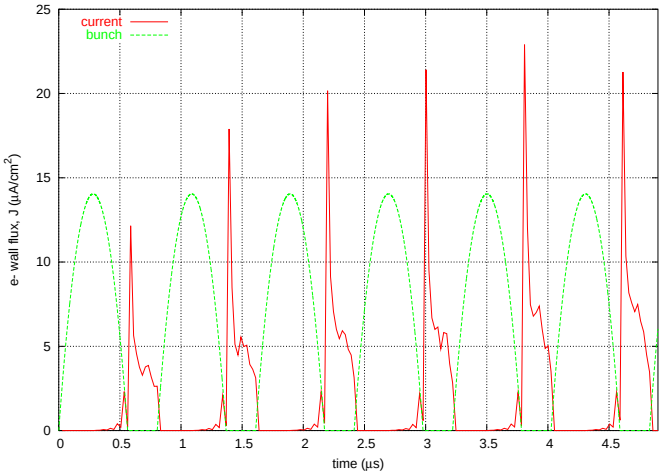

(b) Flux of electrons striking vacuum chamber walls

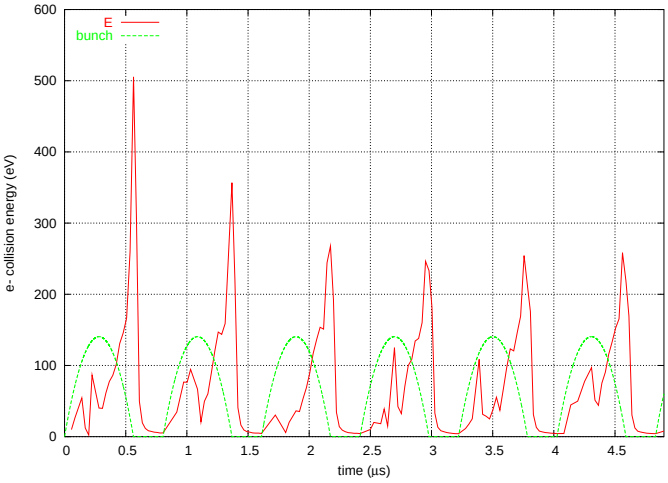

(c) Energy of electrons striking vacuum chamber walls

Figure 2.2.2: Study of Electron Cloud build up in the ESS Accumulator Rings

Figure 2.2.2 shows the results of an initial study into the electron build up during the first few passages of the proton bunch in the ESS accumulator rings. The lower two graphs contain details of the flux and energy distribution of the electrons striking the vacuum chamber walls. Comparative figures for the unstable PSR are an electron density of ~10 nC/m, a wall flux of ~250 μA/cm^2 and a peak collision energy of about 300 eV. Values for ISIS are much lower, for example about 5 μA/cm^2 for the wall flux and 250 eV for the peak electron collision energy.

To assess the problem, a sustained computational and experimental programme has been established, with participants from the USA (BNL, LANL, LBL, ORNL), Europe (CERN, GSI, PSI, RAL) and Japan (KEK). An attempt is being made at RAL to reconcile existing codes worldwide and create a modelling tool containing as many of the known physical effects as possible. An ultimate goal is to include a full electron cloud model in a parallelised rings tracking code. At the same time an experimental programme is being developed at RAL to ascertain the particular features that suppress the instability on ISIS and to identify tests that can be used to benchmark the new codes.

2.3 STRIPPING FOIL TEMPERATURES

Each ring contains a rectangular injection foil, 42.5 mm wide and 14.3 mm high, with mass per unit area of 540 μg cm^{-2} corresponding to a thickness of 3.5 μm for graphite. 2.34×10^{14} H^- ions are stripped of two electrons over a 470 μs pulse duration (583 revolutions) at a repetition rate of 50 Hz. Once in the ring, some circulating protons pass again through the foil, though optimisation studies and tracking described in the previous technical report have reduced this to approximately one passage per particle.

The injected H^- ions, stripped electrons and re-circulating protons scatter in the foil and generate large temperature rises through atomic excitations and ionisation. Radiation cooling reduces the temperature between pulses and a constant peak temperature is reached after the passage of approximately seven pulses

Heating and cooling of the ESS foil have been simulated in a computer program developed from that described in [Duke, 1996]. The main changes have related to improved handling of input data and conversion to run on a fast parallel Linux cluster. However, the principles remain the same. Options have been included to use input H^- beam and re-circulating proton distributions based on injection tracking studies or to use model input distributions. The latter have been used mainly for analytical studies of the effect on the peak temperature of changing parameters such as the H^- beam dimensions, the position of the spot on the foil and the number of proton traversals and injection turns. These have served to confirm the necessity of dividing the total number of protons between two accumulator rings and underline the advantages of the reduced number of injection turns resulting from the larger ring radius.

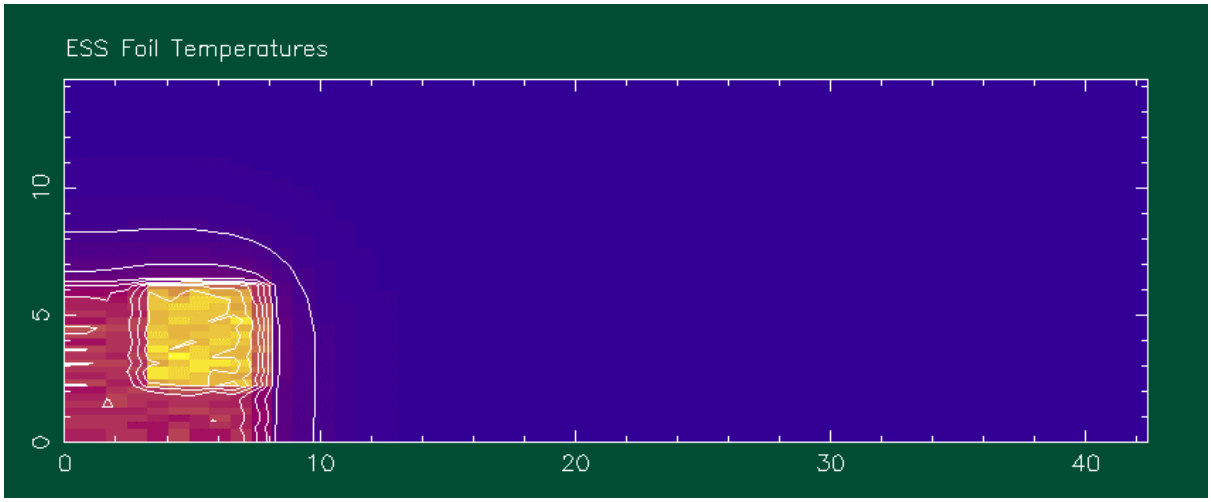

Figure 2.3.1: Heat distribution across ESS foil

With tracking simulations suggesting only one proton foil traversal on average after the initial H^- transit, the foil heating code indicates a peak temperature for graphite of 1880°K (Fig. 2.3.1). This is well below the melting point of 3823°K and suggests the temperature increase is no longer the problem first thought. However, practical tests remain to be undertaken and for this the ESS study can look to work at the SNS where the numbers of

injection turns and proton traversals are much higher and concerns over foil lifetime much more severe.

REFERENCES

[Duke, 1996] J P Duke et al
Stripping Foil Temperatures in the European Spallation Source.
Proceedings of the 5th European Particle Accelerator Conference EPAC'06, Sitges, June 1996

[Macek, 2001] R Macek at al
Recent Experimental Studies of the Electron Cloud at the LANL PSR.
Electron-Proton Instability Workshop, KEK, October 2001

[Rees, 1999] G H Rees
Aspects of Beam Stability at ISIS.
Workshop on Instabilities in High Intensity Hadron Beams in Rings, Upton, NY, June 1999